Inorg. Chem. **2006**, *45*, 5027–5033

Structural Basis for the Phase Switching of Bisaminecopper(II) Cations at the Thermal Limits of Lattice Stability

Panče Naumov,*[,†,‡,§] Kenji Sakurai,[||] Toru Asaka,[⊥] Alexei A. Belik,[†] Shin-ichi Adachi,[‡,#] Junichi Takahashi,[‡,#] and Shin-ya Koshihara[‡,#,○]

International Center for Young Scientists, National Institute for Materials Science, 1-1 Namiki, Tsukuba, Ibaraki 305-0044, Japan, Exploratory Research for Advanced Technology (ERATO), 4-1-8 Honcho, Kawaguchi, Saitama 332-0012, Japan, Institute of Chemistry, Faculty of Science, Sts. Cyril and Methodius University, Arhimedova 5, MK-1000 Skopje, Macedonia, X-ray Physics Group, Materials Engineering Laboratory, National Institute for Materials Science, 1-2-1 Sengen, Tsukuba, Ibaraki 305-0047, Japan, HVEMS, National Institute for Materials Science, 1-1 Namiki, Tsukuba, Ibaraki 305-0044, Japan, High Energy Accelerator Research Organization (KEK), 1-1 Oho, Tsukuba, Ibaraki 305-0801, Japan, and Department of Materials Science, Tokyo Institute of Technology, 1-12-1 Ookayama, Meguro, Tokyo 152-8551, Japan

Received January 19, 2006

The structural grounds of the decrease of point and lattice symmetries coupled with switching of the exchange interaction in single crystals of a highly strained, coordinationally unsaturated bisdiaminecopper(II) cation are described. The combined magnetic susceptibility and X-ray diffraction results indicate that the interplay between the inherent vibronic instability and ligand-field strain imposed by moderately flexible, coordinationally shielding ligands enables effective switching of the pseudo-Jahn–Teller d^9 centers between states with different exchange interaction in the low-temperature regime and valence orbital orientation and coordination geometry in the high-temperature regime. Within the low-temperature hysteresis region, the phase transition can also be induced by excitation of the ligand-to-metal charge-transfer bands, resulting in overall shrinkage of the lattice. The compound is a prototype of weakly electronically coupled one-dimensional Jahn–Teller systems, which can undergo phase transitions induced by light, in addition to heating, cooling, and change of pressure, and it represents a prospective basis for the design of switching materials capable of multimode external control.

Introduction

The preparation of novel materials with physical properties that can be efficiently controlled by light is one of the main goals of modern materials science. Systems with photocontrollable magnetism, spin, oxidation-state, or other electronic properties are important as media for storage of information using light as a tool for recording/reading.[1−3] Nonlinear molecules with a partially filled set of degenerate orbitals are inherently Jahn−Teller (JT) unstable,[4−6] an effect that is considered to underpin important phenomena such as high-temperature superconductivity[7] and colossal magnetoresistance.[8] The potentials of JT instability for switching of the metal−ligand distances with pressure and IR radiation have

* To whom correspondence should be addressed at the National Institute for Materials Science. E-mail: naumov.pance@nims.go.jp. Tel.: +81-29-851-3354. Fax: +81-29-851-4706.

[†] International Center for Young Scientists, National Institute for Materials Science.

[‡] ERATO.

[§] Sts. Cyril and Methodius University.

[||] X-ray Physics Group, Materials Engineering Laboratory, National Institute for Materials Science.

[⊥] HVEMS, National Institute for Materials Science.

[#] High Energy Accelerator Research Organization (KEK).

[○] Tokyo Institute of Technology.

(1) Sato, O. *J. Photochem. Photobiol., C* **2004**, *5*, 203.

(2) (a) Gütlich, P.; Hauser, A.; Spiering, H. *Angew. Chem., Int. Ed. Engl.* **1994**, *33*, 2024. (b) Gütlich, P.; Garcia, Y.; Woike, T. *Coord. Chem. Rev.* **2001**, *219*−*221*, 839.

(3) Bonhommeau, S.; Molnár, G.; Galet, A.; Zwick, A.; Real, J.-A.; McGarvey, J. J.; Bousseksou, A. *Angew. Chem., Int. Ed.* **2005**, *26*, 3943.

(4) Kaplan, M. D.; Vekhter, B. G. *Cooperative Phenomena in Jahn*−*Teller Crystals*; Plenum Press: New York, 1995.

(5) Bersuker, I. B. *The Jahn*−*Teller Effect and Vibronic Interactions in Modern Chemistry*; Plenum Press: New York, 1984.

(6) Falvello, L. R. *J. Chem. Soc., Dalton Trans.* **1997**, 4463.

(7) Fil, D. V.; Tokar, O. I.; Shelankov, A. L.; Weber, W. *Phys Rev.* **1992**, *B45*, 5633.

(8) Jin, S.; Tiefel, T. H.; McCormack, M.; Fastnacht, R. A.; Ramesh, R.; Chen, L. H. *Science* **1994**, *264*, 413.

10.1021/ic060110s CCC: $33.50
Published on Web 05/25/2006

already been demonstrated on Tutton salts.[9] It has been suggested that the JT effect is also responsible for the structural differences between some thermally induced phases and phases obtained by light-induced excited spin state trapping.[10] In principle, an increase of the lattice degrees of freedom by the creation of additional, light-induced JT phases in a vibronically coupled system would increase its overall multistability. Switching dynamics between the limiting structural configurations of such a system will be determined by the nonadiabatic vibronic mixing of its electronic states. Hence, there are expected to be very rapid macrostructural responses to externally seeded microperturbations, which if combined with the multistability of the system, have the potential for the design of ultrafast high-density memories. In this study, a pseudo-JT crystal composed of d_{z^2} arrays of highly strained, coordinationally unsaturated copper(II) ions is utilized as a potentially light-susceptible, electronically weakly coupled medium for which significant structural perturbations are expected upon excitation. The steady-state version of the in situ photodiffraction, a technique developed recently for direct analysis of short-lived or metastable photoinduced species,[11] was employed to demonstrate that, in addition to heating and pressure, the pseudo-JT centers of this system can be switched by cooling and photoexcitation.

As a coordinationally unsaturated unit, the square-planar *trans*-bis(*N*,*N*-diethylethylenediamine)copper(II) (CuDED) cation in its perchlorate salt[12] was selected.[13,14] The bulky *gem*-dialkyldiamine ligands play multiple structural roles: first, they determine the square-planar geometry by shielding the dangling apical metal valences from the approach of the counteranions beyond nonbonded distances; second, they effectively space out the metal ions, preventing dimerization; and third, they provide significant yet limited flexibility for distortions of the primary coordination sphere. The resulting instability can be compensated for by pressure[15] or by heating above 317.6 K,[16] where the internal strain outweighs the energy gain from the electronic state ordering and the respective lattice distortions, resulting in spontaneous transition of the triclinic lattice ($P\bar{1}$, phase A) to a monoclinic one ($I2$, phase B) with doubled volume and tetrahedral distortion of the ligand plane.[17,18] The angular overlap model[16] attributes nearly equal contributions from the puckering and d-orbital energies to the enthalpy gain of the A ↔ B transition. The ligand-field energy change decreases the $(d_{yz},d_{xz})-d_{x^2-y^2}$ gap, resulting in a red shift of the absorption maximum of B for about 1400 cm^{-1} into the violet region, which can be visually observed as a remarkable change of the color from dark red to violet above 319 K (Figure 1).

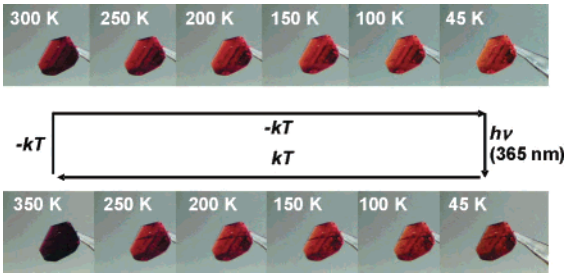

Figure 1. Color change of a single crystal of $(CuDED)(ClO_4)_2$ accompanying the thermochromic and photochromic phase transitions. The arrows indicate the order of the temperature/light treatment.

Results

Figure 2 represents the results of structural analysis of the phase transition A ↔ B by in situ X-ray diffraction.[19] Slices of the three-dimensional difference Fourier electron density maps through the ring atoms show that, above the transition point, the residual electron density corresponding to the atoms N1 and C2 is elongated quasi-normal to the chelate ring, whereas that of C1 and N2 (the latter is not shown) remains more symmetric. Correspondingly, the ellipsoids of anisotropic displacement of N1 and C2 obtained in the least-squares refinement are deformed more than those of C1 and N2. Therefore, the ring in B puckers mainly along the C1−N2 diagonal (Figure 2D,E). The approximate occupancies of the disordered components of C2 and N1 in B amount to (0.64, 0.36) and (0.80, 0.20), respectively. The disorder

(9) (a) Simmons, C. J.; Hitchman, M. A.; Stratemeier, H.; Schultz, A. J. *J. Am. Chem. Soc*. **1993**, *115*, 11304. (b) Iversen, B. B.; Larsen, F. K.; Reynolds, P. A.; Figgis, B. N. *Acta Chem. Scand*. **1994**, *48*, 800. (c) Schultz, A. J.; Hitchman, A. M.; Jorgensen, J. D.; Lukin, S.; Radaelli, P. G.; Simmons, C. J.; Stratemeier, H. *Inorg. Chem*. **1997**, *36*, 3382. (d) Chen, Z.; Fei, S.; Strauss, H. L. *J. Am. Chem. Soc*. **1998**, *120*, 8789. (e) Augustyniak, M. A.; Krupski, L. *Chem. Phys. Lett*. **1999**, *311*, 126.

(10) (a) Sato, O. *Acc. Chem. Res*. **2003**, *36*, 692. (b) Nakamoto, A.; Kojima, N.; Liu, X. J.; Moritomo, Y.; Nakamura, A. *Polyhedron* **2005**, *24*, 2909. (c) Letard, J. F.; Guionneau, P.; Nguyen, O.; Costa, J. S.; Marcen, S.; Chastanet, G.; Marchivie, M.; Goux-Capes, L. *Chem.—Eur. J*. **2005**, *11*, 4582. (d) Gütlich, P. *Top. Curr. Chem*. **2004**, *234*, 231. (e) Marchivie, M.; Guionneau, P.; Letard J. F.; Chasseau, D.; Howard, J. A. K. *J. Phys. Chem. Solids* **2004**, *65*, 17. (f) Nakamoto, A.; Ono, Y.; Kojima, N.; Matsumura, D.; Yokoyama, T.; Liu, X. J.; Moritomo, Y. *Synth. Met*. **2003**, *137*, 1219. (g) Moliner, N.; Salmon, L.; Capes, L.; Munoz, M. C.; Letard, J. E.; Bousseksou, A.; Tuchangues, J. P.; McGarvey, J. J.; Dennis, A. C.; Castro, M.; Burriel, R.; Real, J. A. *J. Phys. Chem*. **2002**, *B106*, 4276. (h) Harimanow, L. S.; Sugiyarto, K. H.; Craig, D. C.; Scudder, M. L.; Goodwin, H. A. *Aust. J. Chem*. **1999**, *52*, 109. (i) Buchen, T.; Schollmeyer, D.; Gütlich, P. *Inorg. Chem*. **1996**, *35*, 155. (j) Gütlich, P. *Nucl. Instrum. Methods Phys. Res*. **1993**, *76*, 387.

(11) For examples of steady-state and time-resolved photodiffraction, see: (a) Techert, S.; Schotte, F.; Wulff, M. *Phys. Rev. Lett*. **2001**, *86*, 2030. (b) Collet, E.; Lemée-Cailleau, M.-H.; Buron-Le Cointe, M.; Cailleau, H.; Wulff, M.; Luty, T.; Koshihara, S.; Meyer, M.; Toupet, L.; Rabiller, P.; Techert, S. *Science* **2003**, *300*, 612. (c) Guérin, L.; Collet, E.; Lemée-Cailleau, M.-H.; Buron-Le Cointe, M.; Cailleau, H.; Plech, A.; Wulff, M.; Koshihara, S.; Luty, T. *Chem. Phys*. **2004**, *299*, 163.

(12) The details of the synthesis were deposited as Supporting Information.

(13) Takahashi, K.; Nakajima, R.; Gu, Z.; Yoshiki, H.; Fujishima, A.; Sato, O. *Chem. Commun*. **2002**, 1578.

(14) Yokoyama, T.; Takahashi, K.; Sato, O. *Phys. Rev*. **2003**, *B67*, 172104.

(15) Ferraro, J. R.; Basile, L. J.; Garcia-Ineguez, L. R.; Paoletti, P.; Fabrizzi, L. *Inorg. Chem*. **1976**, *15*, 2342.

(16) Nishimori, A.; Sorai, M.; Schmitt, E. A.; Hendrickson, D. A. *J. Coord. Chem*. **1996**, *37*, 327.

(17) Grenthe, I.; Paoletti, P.; Sandström, M.; Glikberg, S. *Inorg. Chem*. **1979**, *18*, 2687.

(18) (a) Takahashi, K.; Nakajima, R.; Gu, Z.; Yoshiki, H.; Fujishima, A.; Sato, O. *Chem. Commun*. **2002**, 1578. (b) Naumov, P.; Sakurai, K.; Asaka, T.; Belik, A. A.; Adachi, S.; Takahashi, J.; Koshihara, S. *Chem. Commun*. **2006**, 1491. (c) Naumov, P.; Sakurai, K.; Asaka, T.; Belik, A. A.; Adachi, S.; Takahashi, J.; Koshihara, S. *Eur. J. Inorg. Chem*. **2006**, 1345.

(19) The structures of both low-temperature (A, 293 and 313 K) and high-temperature (B, 319 K) phases were determined in situ, in two independent experiments from different temperature-controlled single crystals. The details were deposited as Supporting Information.

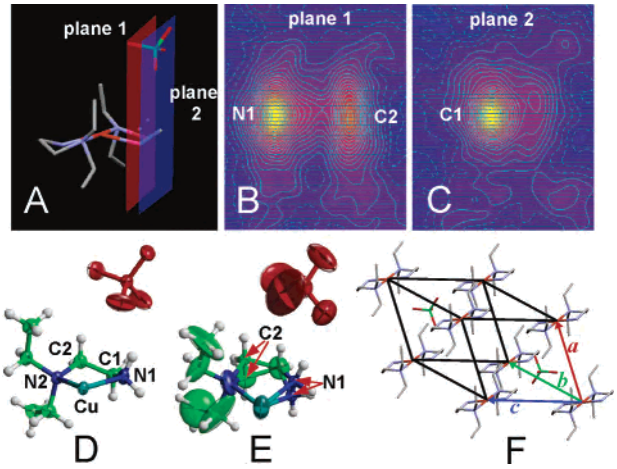

Figure 2. (A) Quasi-orthogonal (with respect to the chelate ring) planes probing the difference electron density through N1 and C2 (plane 1) and C1 (plane 2). (B) Experimental difference Fourier electron density in plane 1 for a molecular model refined without atoms N1 and C2. (C) Experimental difference Fourier electron density in plane 2 for a molecular model refined without atom C1. (D) Thermal ellipsoid plots of the half formula unit of phase A. (E) Thermal ellipsoid plots of the half formula unit of phase B (both disordered components of both C2 and N1 are shown). (F) Crystal packing of $(CuDED)(ClO_4)_2$ in phase A.

caused by ring oscillations is transferred to the alkyl termini (Figure 2E), but because of the significant thermal contributions to the vibrational motions at these temperatures, the disorder of the alkyl positions is not readily resolvable in the three-dimensional difference Fourier maps. The orientation and position of the perchlorate ions are also altered: from 293 to 319 K, the chlorine atom closest to the copper shifts about 320 pm away because of the increased overall uniaxial rotations of the anion (Figure 2E).

The magnetic susceptibility of $(CuDED)(ClO_4)_2$ single crystals cycled thermally in the dark below the phase transition A ↔ B (2−300 K) exhibits reproducible anomalies at low temperature (Figure 3A).[20] As shown in the inset of Figure 3A, upon cooling (↓) from ambient temperature, a single-step transition occurs at 48 K ($T_{\downarrow}$), with onset at 60 K. During subsequent heating (↑), the susceptibility is recovered in two steps between 25 and 57 K, at 30 K ($T_{\uparrow,1}$) and 52 K ($T_{\uparrow,2}$). The hysteresis is reproducible by repeated thermal cycling with the magnetic field vector oriented perpendicular to each of the three crystal faces. In the case of a powder sample, the effect appears only as a slight change of the slope of the magnetic susceptibility curve because of the similarity of the effective moments (μ_{eff}) in the two regimes. The modified Curie−Weiss (CW) model reveals a change of the exchange interaction at $T_{\downarrow}$ from the high-temperature ferromagnetic regime I, phase A (80−290 K), to a low-temperature antiferromagnetic regime II, phase C (2−28 K), with hysteresis in the range 25−55 K (Table 1). As shown in Figure 4, the two steps at $T_{\uparrow,1}$ and $T_{\uparrow,2}$ resolved upon heating reveal that the one-step transition at $T_{\downarrow}$ upon

(20) Magnetic susceptibilities, $\chi = M/H$, were measured in a settle mode, with a SQUID magnetometer (Quantum Design, MPMS) between 2 and 300 K in an applied field of 10 kOe [1 Oe = $(10^3/4\pi)$ A/m]. All of the measurements started from 300 K. The temperature steps were 1 K between 2 and 100 K and 5 K between 105 and 300 K. The heating/cooling rate was 10 K/min between the steps.

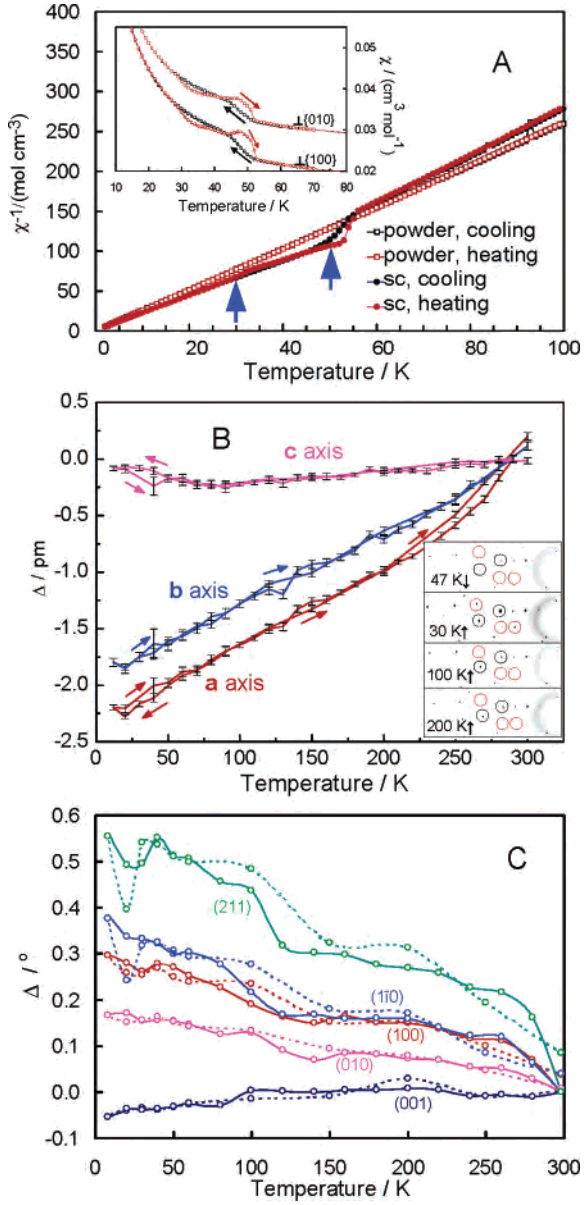

Figure 3. Thermal effects on the structure of $(CuDED)(ClO_4)_2$ below ambient temperature. (A) The region 2−100 K of the magnetic susceptibility of a single crystal (sc, filled circles) and a powder (open circles) cycled between 2 and 300 K. The two transition temperatures, $T_{\uparrow,1}$ and $T_{\uparrow,2}$, are denoted with blue arrows. Inset: hysteresis in the magnetic susceptibility of sc recorded with the magnetic field nearly perpendicular to the faces {010} (one cycle) and {100} (two overlapped cycles, showing the reproducibility of the transition). (B) Cyclic temperature profiles of the cell axes from sc X-ray data. $\Delta(a)/\text{Å} = a/\text{Å} - 8.0959$, $\Delta(b)/\text{Å} = b/\text{Å} - 8.7312$, and $\Delta(c)/\text{Å} = c/\text{Å} - 9.7868$ (subtracted values refer to $T = 290$ K). Inset: Temperature effects on the high-resolution sc diffraction pattern. (C) Temperature profiles by cooling (solid lines) and subsequent heating (broken lines) of the positions of several selected reflections in the powder diffraction pattern. The error bars are equal for all points and amount to ±0.01°.

cooling from region I to region II involves two simultaneous processes. From the two steps upon heating, the one at $T_{\uparrow,1}$ probably corresponds to switching of the exchange interaction of the antiferromagnetic phase C in region II to an intermediate phase in region III, which by structural change of the lattice at $T_{\uparrow,2}$ is transformed back to the original lattice A in region I.

Below the high-temperature transition (A ↔ B), the continuous distortion of the ligand field and the respective

Table 1. Fitted Parameters for $\chi^{-1}(T)$[a]

quantity	single crystal	powder
temperature range (K)	2−28	2−28
χ_0 (cm^3/mol of Cu)	$-1.0(4) \times 10^{-5}$	$-3(2) \times 10^{-5}$
μ_{eff} (μ_B), g	1.916(2), 2.2124	1.7692(14), 2.0429
θ (K)	−0.467(15)	−0.162(9)
temperature range (K)	80−290	80−290
χ_0 (cm^3/mol of Cu)	$-3.36(3) \times 10^{-4}$	$-4.26(9) \times 10^{-5}$
μ_{eff} (μ_B), g	1.743(3), 2.0126	1.7427(8), 2.0123
θ (K)	2.6(3)	1.81(7)

[a] The modified CW law of the form $\chi(T) = \chi_0 + \mu_{eff}^2 N_A[3k_B(T - \theta)]^{-1}$ was used, where χ_0 is the temperature-independent term, μ_{eff} is the effective magnetic moment, N_A is Avogadro's number, k_B is Boltzmann's constant, θ is the Weiss constant, and g is the g value.

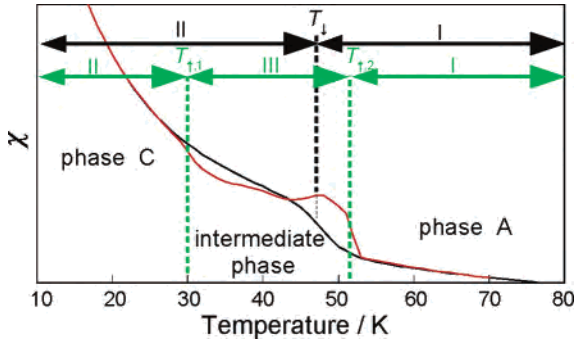

Figure 4. Regions I (phase A), II (phase C), and III (intermediate phase) in the course of the low-temperature phase transition of $(CuDED)(ClO_4)_2$ upon cooling (black) and subsequent heating (red) monitored by the temperature profile of the single-crystal magnetic susceptibility.

shift of the visible absorption end with temperature can be detected visually as a gradual color change from dark red at 293 K to orange below 100 K (Figure 1). The thermal hysteresis of the cell volume below $T_{\downarrow}$ is clearly observable in the cell axes a and c of single crystals (Figure 3B) as well as in the reflection positions in the X-ray diffraction pattern of powder samples (Figure 3C; plots of the powder patterns are deposited as Figure S1 in the Supporting Information). As indicated by the thermal profiles of the c axis (Figure 3B) and the reflection (001) (Figure 3C), although the three axes are of similar length [$a = 8.0959(32)$ Å, $b = 8.7312(35)$ Å, and $c = 9.7868(25)$ Å at 290 K], the crystal lattice in both single-crystalline and microcrystalline states experiences strong compression only on the faces ac and bc, while the shrinkage along c is compensated for by expansion counterforce, which becomes dominant below 90 K. The presence of only one formula unit per unit cell in A ($Z = 1$) and the coincidence of lattice nodes with the metal centers allow straightforward interpretation of the effect: only two out of the three lattice degrees of freedom are thermally active, those along the a axis (perpendicular to the coordination plane) and b axis (in the direction of the unsubstituted nitrogen atom of the coordination plane; Figure 2F). The anomalous uniaxial expansion along c below 90 K results in the low-temperature spin−lattice transformation to phase C. The symmetry decrease related to the transition is reflected in the high-resolution X-ray diffraction pattern of a single crystal obtained by using synchrotron radiation[21] as elongation, partial splitting and changes of the relative peak intensity, and appearance of new peaks around 30 K (the inset in Figure 3B; deposited as an expanded version as Figure S2 in the Supporting Information). Upon slow heating, the peak intensities of C gradually decrease, partially split peaks merge back, and the original pattern is recovered, demonstrating reversibility of the transition. Traces of phase C are detectable up to 150−200 K.

For aged powdered samples, pulsed-heat relaxation (this study) and adiabatic[16] heat capacity measurements showed the absence of notable thermal effects. Nevertheless, the thermal hysteresis of the lattice strain coupled with a change of the exchange interaction of powder samples below 60 K is clearly evidenced by the diffraction pattern (Figure 3C) and the magnetic susceptibility (Table 1).[22] In view of the influence of the pressure on the structure,[15] it is suggested that the sample history causes slightly different behavior around the hysteresis region in single-crystalline and microcrystalline states: because of the pressure that was applied during the powdering, the lattice strain in a slowly cooled powder sample is released by smaller changes of the lattice structure. On the contrary, the long-range order in virgin single crystals enables effective symmetry switching of larger crystal domains, which influences the spin-exchange process.

The UV/visible spectrum of solid $(CuDED)(ClO_4)_2$ is dominated by a broad red absorption band $(d_{yz},d_{xz})-d_{x^2-y^2}$ centered around 510 nm and ligand-to-metal charge-transfer (LMCT) bands in the region 200−400 nm (maxima at 305 and 255 nm). Excitation of the LMCT transitions in the solid state with a CW He−Cd laser at 354 nm at room temperature results in strong fluorescence at 575 nm. Similarly to the visible absorption band at 510 nm, the broad emission band at 575 nm is sensitive to the temperature, and it is structurized and shifted to 645 nm at 125 K. The presence of the emission band indicates that the metal centers are sufficiently distant for significant deactivation of any eventual pathways for nonradiative decay. The trapping of the excitation energy within the individual metal centers seems to be crucial for induction of the photoinduced transformation described below. Mostly because of the combination of internal strain and lattice instability and to some extent because of the weak

(21) Beamline NW2 at Photon Factory−Advanced Ring (Tsukuba, Japan), 30 mA, 6.5 GeV, $\lambda = 0.6889$ Å, single-bunch mode, bunch duration 100 ps, beam size 0.26 × 0.60 mm (the details of the beamline are explained in: Mori, T.; Nomura, M.; Adachi, H.; Uchida, Y.; Toyoshima, A.; Yamamoto, S.; Tsuchiya, K.; Shioya, T.; Kawata, *8th Int. Conf. Synchr. Rad. Instrum., Am. Inst. Phys. Conf. Proc.* **2003**, *705*, 255). The data were collected on a three-circle diffractometer equipped with a CCD detector (Rigaku/MSC Mercury), by ω scans in horizontal geometry, with steps of 2° and an exposure time of 5 s. The crystal samples used were of dimensions 100−200 μm at each side. Careful temperature control and good crystal quality proved to be crucial for the preservation of the crystal integrity during the phase transition. The crystal was cooled by a helium flow of an open-type cryostat, and the temperature was corrected for differences between the sensor and the sample position measured independently.

(22) The powder diffraction patterns are deposited as Supporting Information (Figure S1). Probably because of the applied pressure, significant changes in the diffraction pattern were observed immediately after the powdering using a mortar and pestle (the grain size was not controlled). Hence, prior to the measurement, all powdered samples were aged for 1 day in the dark at ambient temperature. The patterns were recorded in the 5−60° region of 2θ, with steps of 0.02° (0.002° in the case of the photoirradiation experiments) and an exposure time of 5 s, with germanium-monochromatized Cu Kα radiation (40 kV, 50 mA), using an M03XHF MAC Science diffractometer.

electronic coupling along the cationic chains, it is expected that photoinduced local perturbations of the structure of individual metal centers in the bistability region are feasible and, if the cooperative structural processes are operative, they might influence the long-range structural order.

To test such a hypothesis, the effect of photoexcitation on the structure was examined with a specially designed system for temperature-controlled powder photodiffraction on a laboratory scale (Figure S3, deposited in the Supporting Information). Upon 365-nm flash excitation of the LMCT bands, the strong reflections shift 0.04° on average, most of them to the higher 2θ side, with various trends of the intensity change (Figure 5A)[23] and a remarkable color change from bright orange to violet. The direction of the peak shift[24] and the long data collection time relative to the irradiation ensure that the respective cell shrinkage is not due to heating effects but to the creation of a long-lived photoinduced ground state. The overall effect of the excitation on the lattice is analogous to cooling of the crystal. The temperature dependence of the photoinduced structural change, monitored by the position of the $(1\bar{1}0)$ reflection (Figure 5B), showed that the photoexcitation strongly affects the lattice upon cooling within the hysteresis region III, where phase C and the intermediate phase exist upon cooling and heating, respectively. From the magnitude of the shift, it is concluded that the largest structural change occurs at 45 K, right after the transition of A to C upon cooling has been completed (Figure 4). This is an indication that the excitation induces the transition from the low-temperature phase C, obtained in situ from cooled A, to the intermediate phase between C and A, close to the transition point. As shown in Figure 5B, excitation below 30 K is less effective and results in a qualitatively different structural change, which was confirmed by a comparison of the difference patterns in the 2θ region of 5−60°. The photoinduced phase persists at 50 K, but it decays by thermal annealing at higher temperatures or by irradiation with visible light. In the case of single crystals, a flash of UV light affects the lattice around 50 K (↓) and in the region 40−60 K (↑), as exemplified by the *c* axis in Figure 5B. Steady-state UV irradiation alters significantly the intensities and positions of the strong reflections, indicating that the excitation affects the bulk structure.[21,25] Therefore, the diffraction experiments are conclusive that, within and around the bistable region III, the photoexcitation significantly affects the crystal and electronic structure, particularly of the coupled cationic centers.

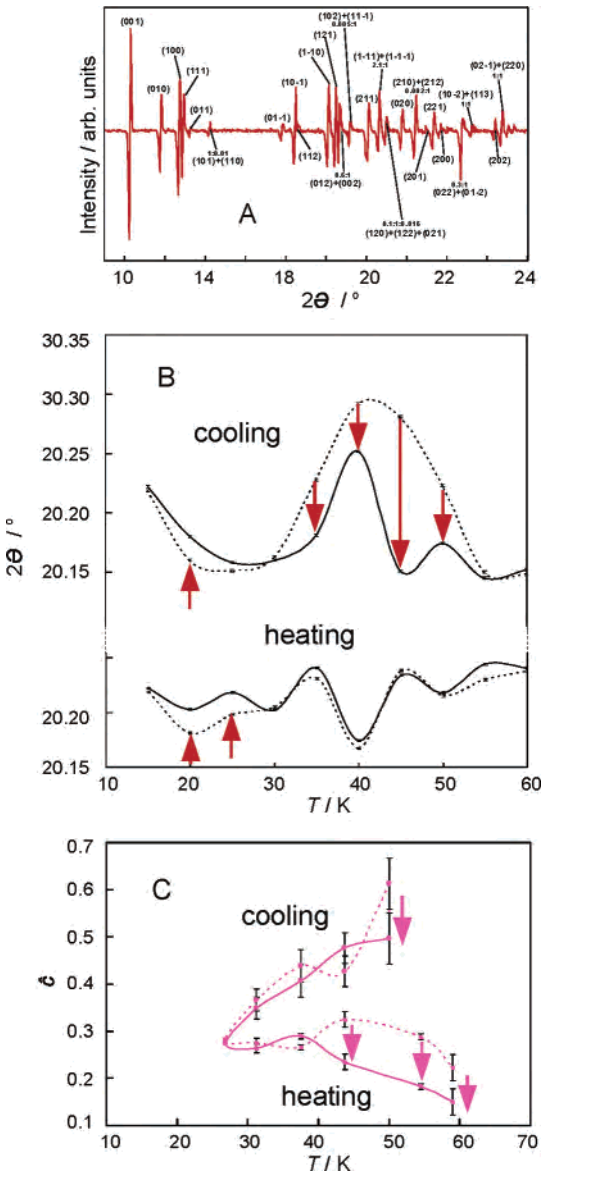

Figure 5. Excitation effects on $(CuDED)(ClO_4)_2$ at low temperature. (A) Difference diffraction pattern (after − before) of a UV-flash-excited (λ_{max} = 365 nm, 0.1 s) powder sample with peak assignments based on the simulated low-temperature single-crystal diffraction data. (B) Temperature profile of the fitted maximum of the reflection $(1\bar{1}0)$ before (dashed lines) and after (solid lines) 1 s of excitation by 365-nm light. The sample was annealed at 300 K between each of the two temperatures. In the case of partial splitting, the average value of the fitted components was plotted. (C) Temperature profile of the normalized *c* axis, $c = 10(c/\text{Å} - 9.6937) + 0.1$ before (dashed line) and after (solid line) UV excitation (λ_{max} = 365 nm, 1 s). The sample was excited at each temperature, without thermal annealing between the consecutive temperature points.

Discussion

To correlate the structure to the temperature characteristics of the ambient-temperature thermal phase transitions, $(CuDED)(ClO_4)_2$ was compared with the known phases of the respective tetrafluoroborate, $(CuDED)(BF_4)_2$,[26] and nitrate, $(CuDED)(NO_3)_2$,[27] salts. The inferences open a prospective

(23) The sample was irradiated with double UV output from a 250-W Hg lamp (λ_{max} = 365 nm, SP-7 with internal heat filter, Ushio) in a laboratory-built cryostat for powder photodiffraction with Kapton windows for X-ray and replaceable optics for light irradiation (Figure S3 in the Supporting Information). The heat-filtered UV light was focused by fused-silica biconvex UV lenses through UV-transparent quartz windows. The sample was exposed, in quasi-perpendicular geometry, to single flashes with a duration of 0.1 or 1 s.

(24) The average peak shift of 0.04° is comparable with values reported for excited/ground state mixtures of paddlewheel binuclear platinum anions with long-lived excited states: (a) Ikagawa, T.; Okamura, T.; Otsuka, T.; Kaizu, Y. *Chem. Lett*. **1997**, 829. (b) Yasuda, N.; Uekusa, H.; Ohashi, Y. *J. Chem. Soc. Jpn*. **2004**, *77*, 933.

(25) For example, upon excitation with polychromatic light (365 nm), the relative intensities of the reflections $(10\bar{1})$, $(1\bar{1}0)$, $(1\bar{1}2)$, (201), (222), $(\bar{1}\,\bar{1}0)$, and $(\bar{2}02)$ are changed as +133, −67, +10, −82, −41, −64, and −10%, respectively (SR data).

(26) Narayanan, B.; Bhadbhade, M. M. *J. Coord. Chem*. **1998**, *46*, 115.

(27) Naumov, P.; Belik, A. A.; Nukui, A.; Tanaka, M.; Sakurai, K. *Chem. Mater*., submitted for publication.

Table 2. Thermal Phase Transitions and Relevant Structural Parameters of the Perchlorate, Tetrafluoroborate, and Nitrate Salts of CuDED in Their High-Temperature (HT), Room-Temperature (RT), and Low-Temperature (LT) Phases

parameter	compound		
	$(CuDED)(ClO_4)_2$	$(CuDED)(BF_4)_2$[a]	$(CuDED)(NO_3)_2$[b]
color of the HT phase	violet	violet	red-violet
cryst syst, space group of the HT phase	monoclinic, $I2$	monoclinic, $I2$[c]	unknown
temp and cell param of the LT phase (phase B)	$T = 319(2)$ K $a = 9.955(2)$ Å $b = 8.383(2)$ Å $c = 13.289(3)$ Å $\alpha = 90°$ $\beta = 97.437(2)°$ $\gamma = 90°$ $V = 1099.6(3)$ Å^3		
T of the HT phase transition[d]	317.6 K	302.6 K	348−371 K[f]
color of the RT phase	red	red	red
cryst syst, space group of the RT phase	triclinic, $P\bar{1}$	triclinic, $P\bar{1}$	monoclinic, $P2_1/n$
temp and cell param of the RT phase (phase A)	$T = 293$ K $a = 8.093(3)$ Å $b = 8.744(2)$ Å $c = 9.769(2)$ Å $\alpha = 65.289(2)°$ $\beta = 66.001(2)°$ $\gamma = 63.483(2)°$ $V = 540.9(2)$ Å^3	$T = 295$ K $a = 8.0136(9)$ Å $b = 8.6410(10)$ Å $c = 9.7196(7)$ Å $\alpha = 65.735(11)°$ $\beta = 66.498(8)°$ $\gamma = 63.486(13)°$ $V = 529.6(9)$ Å^3	$T = 200$ K $a = 8.186(1)$ Å $b = 12.644(2)$ Å $c = 9.677(2)$ Å $\alpha = 90°$ $\beta = 105.942(2)°$ $\gamma = 90°$ $V = 963.1(2)$ Å^3
T of the LT phase transition[e]	25−55 K[f]	<80 K	42−52 K[f]
color of the LT phase (phase C)	orange	orange	orange

[a] The room-temperature data for the complex were taken from ref 26. [b] Measurements were performed on anhydrous crystals obtained by drying of the fresh crystals in a vacuum. [c] The refinement of the structure from powder diffraction data is in progress [d] Determined by differential scanning calorimetry. [e] Determined by magnetic susceptibility measurements. [f] With thermal hysteresis.

for tuning of the phase transition temperature by introducing small structural changes.

Both temperature and pressure induce significant strain in the crystal lattices of all three compounds. Applying pressure by pressing or even during grinding in a mortar results in readily observable piezochromism and a color change from red to violet. Because of the gradual thermochromic phase transition to the high-temperature phases, heating of all three compounds also results in an apparent color change, as elaborated above in the case of the perchlorate salt. The temperatures of the phase transitions are listed together with the results of the crystallographic analysis of ambient-temperature phases A and high-temperature phases B in Table 2. The order of transition temperatures is $(CuDED)(BF_4)_2 < (CuDED)(ClO_4)_2 \ll (CuDED)(NO_3)_2$, with the $(CuDED)(BF_4)_2$ crystals undergoing the transition and turning violet already at ambient temperature, immediately after separation from the solution.

At ambient temperature, the crystals of $(CuDED)(ClO_4)_2$ and $(CuDED)(BF_4)_2$ are triclinic, while those of $(CuDED)(NO_3)_2$ are monoclinic. As shown by the packing diagrams in Figure 6, the coordination plane in the triclinic $(CuDED)(ClO_4)_2$ crystal is nearly perpendicular to the cation stacking direction, which coincides with the a axis. The d_{z^2} orbitals of the neighboring metal centers are separated at a Cu- - -Cu = a distance of 8.09 Å. Similarly to $(CuDED)(ClO_4)_2$, the cations in the isomorphous triclinic $(CuDED)(BF_4)_2$ crystal are translated 8.01 Å along the a axis. In the case of the monoclinic $(CuDED)(NO_3)_2$ crystal of $P2_1/n$ symmetry, the C_i axes of the neighboring cations are not perpendicular to the stacking axis a, but instead they are offset with respect to each other (Figure 6). Although the Cu- - -Cu = a distance of $(CuDED)(NO_3)_2$ of 8.19 Å is only slightly larger than

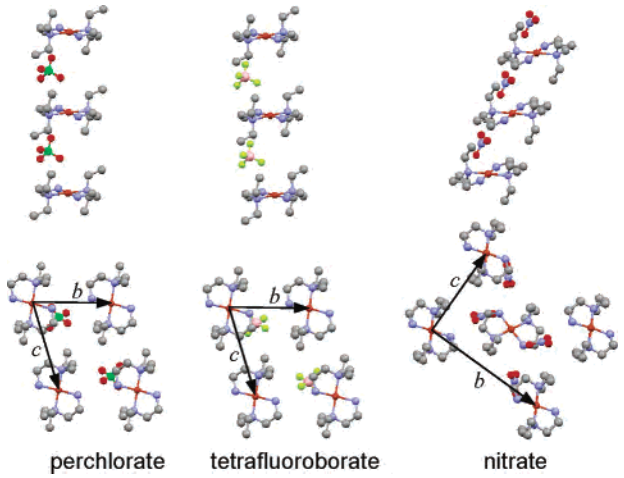

Figure 6. Crystal structures of the room-temperature phases (A phases) of bis(*N*,*N*-diethylethylenediamine)copper(II) tetrafluoroborate, $(CuDED)(BF_4)_2$ ($P\bar{1}$), perchlorate, $(CuDED)(ClO_4)_2$ ($P\bar{1}$), and nitrate, $(CuDED)(NO_3)_2$ ($P2_1/n$).

the respective value in the other two compounds, the phase transition A → B proceeds at a temperature that is 53 and 68 K higher than the respective temperatures of $(CuDED)(ClO_4)_2$ and $(CuDED)(BF_4)_2$. Contrary to the other two compounds, which show hysteresis of the low-temperature transition A ↔ C, $(CuDED)(NO_3)_2$ shows a thermal hysteresis of the *high-temperature* phase transition A ↔ B with a width of 23 K.[27]

The increased temperature of the phase transition of $(CuDED)(NO_3)_2$ with respect to the other two salts is apparently related to the spatial offset of the cations in its structure, dictated by the lattice symmetry. The packing provides larger space for increased ligand librations due to increased thermal excitation, without a change of the site

symmetry of the metal center to high temperatures. Ultimately, the reasons for the different packing and, consequently, for the different transition temperatures of (CuDED)$(ClO_4)_2$ and (CuDED)$(BF_4)_2$, on the one hand, and (CuDED)$(NO_3)_2$, on the other hand, can be traced back to the different anions. In the case of the perchlorate and tetrafluoroborate ions, which have approximately spherical symmetry and can easily reorientate upon thermal activation, the cations can stack above each other at shorter Cu- - -Cu distances. In contrast, in the case of the planar nitrate ion (and probably in the case of similar flat anions such as the carbonate), the anion orientation is not readily affected by the temperature. In principle, it is expected that the planarity of the anions would allow stacking of the cations at even shorter distance. Instead, the repulsive coulombic force between the cations results in an offset of their centers along the stacking axis. The longer intermetal distance and the smaller steric hindrance of the alkyl chains result in a higher temperature of the phase transition. This is purported by the order of temperatures of the high-temperature transition, (CuDED)$(BF_4)_2$ (302.6 K) < (CuDED)$(ClO_4)_2$ (317.6 K) ≪ (CuDED)$(NO_3)_2$ (371 K), which corresponds well with the order of the Cu- - -Cu distances, (CuDED)$(BF_4)_2$ (8.01 Å) < (CuDED)$(ClO_4)_2$ (8.09 Å) < (CuDED)$(NO_3)_2$ (8.19 Å). The temperature of the phase transition is determined by small changes of the structure. In return, it should be possible to change the phase transition within a predetermined temperature range by introduction of small changes to the basic cationic structure.

Conclusions

The weakly electronically coupled planar pseudo-JT cations in the cationic chains of (CuDED)$(ClO_4)_2$ are subject to high internal strain, balanced by a relatively strong, but moderately flexible, ligand field. The lattice can withstand such strain only between 60 and 318 K; it collapses by application of external pressure or by alteration of the internal pressure by heating/cooling out of this temperature range.[28] Above 318 K, the strain is released by tetrahedral distortion of the valence orbital orientation, enhanced ring puckering, disorder of the side ligand chains, and positional and rotational disorder of the counteranion. Below 60 K, switching of the exchange interaction in virgin single crystals from the ferromagnetic to antiferromagnetic regime is related to lowering of the point and lattice symmetries with hysteresis between 25 and 55 K. Solely on the basis of the present experimental data, it seems difficult to state whether the crystallographic phase transition, triggered by the lattice instability, is the reason for the anomaly on the temperature dependence of the magnetic susceptibility or the change of the spin exchange interaction results in the phase transition. Keeping in mind that the magnetic interaction between the metal centers is weak, the first alternative appears more feasible. The comparison of the same cation embedded in slightly different crystal environments proved that two of the factors that determine the temperature of the phase transition, directly or indirectly, are the distance and the relative orientation of the neighbor metal centers.

In the region of low-temperature bistability, the phase transition can also be induced from the excited state, by partial charge transfer, which results in overall shrinkage of the lattice. The creation of the photoinduced phase evidences that, in addition to temperature (heating and cooling) and pressure, the strain release in this and probably in similar coordinationally unsaturated one-dimensional pseudo-JT systems can also be triggered by an external electromagnetic field. The result shows that, even in the case of weak magnetic interactions, the structural instability of the lattice at the limits of its thermal stability can be employed for significant perturbation of the crystal structure by photoexcitation. The possibility of employing the interplay between the JT instability and the ligand-field strain, which is determined by moderate flexibility of the primary coordination sphere, for triggering structural transitions by light, pressure, and temperature paves the way of switching devices capable of multistimulus control.

Acknowledgment. This study was performed through Special Coordination Funds for Promoting Science and Technology from the Ministry of Education, Culture, Sports, Science and Technology of the Japanese Government. The authors thank Prof. Y. Matsui for generously providing the powder diffractometer.

Supporting Information Available: Details of the synthesis and diffraction analyses, powder (Figure S1) and single-crystal (Figure S2) diffraction patterns, setup for powder photodiffraction (Figure S3), and X-ray crystallographic data in CIF format. This material is available free of charge via the Internet at http://pubs.acs.org.

IC060110S

(28) The temperature profiles of the cell parameters in single crystalline and powder states (Figure 3B,C) show an additional anomaly around 120 K. Because the process does not have its counterpart in the magnetic susceptibility and heat capacity results, it probably corresponds to the onset of the first-order high-temperature transition A ↔ B, which is a strongly asymmetric and gradual process, extending into a quasi-continuum on the low-temperature side.